PROCEEDINGS OF SCIENCE

Targeting the conformal window with 4+8 flavors

Rich Brower
Department of Physics, Boston University, Boston, MA, USA
E-mail: brower@bu.edu

Anna Hasenfratz
Department of Physics, University of Colorado Boulder, Boulder, CO, USA
E-mail: Anna.Hasenfratz@colorado.edu

Claudio Rebbi
Department of Physics, Boston University, Boston, MA, USA
E-mail: rebbi@bu.edu

Evan Weinberg*
Department of Physics, Boston University, Boston, MA, USA
E-mail: weinbe2@bu.edu

Oliver Witzel†
Center for Computational Science, Boston University, Boston, MA, USA
E-mail: owitzel@bu.edu

We study the transition between spontaneous chiral symmetry breaking and conformal behavior in the $SU(3)$ theory with multiple fermion flavors. Instead of the traditional approach of changing the number of flavors, we keep the number of fermions fixed but lift the mass of a subset, keeping the remaining fermions near to the massless chiral limit. This way we can interpolate continuously between the conformal and chirally broken dynamics. In particular, we consider four light and eight heavy flavors and investigate the running/walking gauge coupling and the low energy meson spectrum, including the 0^{++} iso-singlet scalar state in this system. Our preliminary data reveal an iso-singlet scalar that is considerably lighter than the pion at large fermion mass but becomes heavier at smaller masses. This behavior is of particular phenomenological interest.

The 32nd International Symposium on Lattice Field Theory,
23-28 June, 2014
Columbia University New York, NY

*Speaker.
†Poster, Present address: School of Physics & Astronomy, The University of Edinburgh, EH9 3FD, UK

PoS(LATTICE2014)254

1. Introduction

The experimental discovery of the Higgs boson at the LHC in 2012 [1, 2] contributed the missing piece of the electroweak sector of the Standard Model but so far we do not have experimental insight into the nature of electroweak symmetry breaking or the origin of the Higgs boson. Given the current experimental constraints, there are two theoretically viable scenarios: supersymmetric extensions of the Standard Model and composite Higgs models. Both would solve the well-known problem that theories with self-interacting scalars require an ultraviolet completion, which is not contained in the Standard Model. In this work we consider composite Higgs models that are based on a new, strongly coupled but chirally broken gauge-fermion sector where the Higgs boson is a fermionic 0^{++} bound state. Composite Higgs models originate from "Technicolor" models [3, 4] which subsequently were supplemented by a mechanism to generate fermion masses ("Extended Technicolor") [5, 6] and later refined to "Walking Technicolor" to satisfy electroweak phenomenological constraints [7, 8].

Any new gauge-fermion system predicts a plethora of new composite states which could be in tension with current experimental findings. Hence any composite Higgs model faces the challenge to predict a bound scalar with the mass and properties of the Higgs boson while all other states are at sufficiently larger mass. A model exhibiting a walking behavior induced by a weakly broken conformal symmetry is conjectured to be a promising candidate with the desired spectral properties. Such a system could be realized by a theory close to an infra-red fixed point (IRFP). In this respect, recent lattice results using the $SU(3)$ gauge group have triggered special interest: Independent groups have reported indications for an infrared fixed point in the theory with 12 fundamental flavors [9–16], and a low mass scalar has been observed in investigations with 8 fundamental flavors [17] or 2 sextet flavors [18].

As exciting these results may be, the above considerations are merely a conjecture offering a possible explanation of electroweak symmetry breaking based on a strongly interacting gauge theory. Much more work is needed to (in)validate such a conjecture. Many models of colors, flavors, and fermion representation will need to be investigated because contrary to QCD, little is known experimentally. Like in the case of QCD, lattice simulations offer the only ab initio non-perturbative tool at present to study these non-Abelian gauge theories from first principles.

Given a gauge group and fermion representation most studies choose the number of fermions such that the system is as close to the conformal window as possible. Such models have the highest likelihood of exhibiting the phenomenologically desired properties i.e. a walking scenario with a light mass iso-singlet scalar. The inherent difficulty is that the number of flavors is an integer and not a continuous variable. There is no guarantee that an integer value is close enough to the IRFP. In this work we report on a novel approach that avoids this inherent difficulty.

In our approach we split the masses of the fermions, keeping some of them near the chiral limit while lifting the mass of the others [19]. Based on the evidence that an $SU(3)$ theory with 12 fundamental flavors exhibits an IRFP and the fact that an $SU(3)$ four flavor theory is chirally broken, QCD like, we chose to study a system with $N_\ell = 4$ light and $N_h = 8$ heavy flavors. We keep the N_ℓ light flavors near the chiral limit, i.e., $m_\ell \approx 0$ and give the N_h heavy flavors a variable mass with $m_h \geq m_\ell$. This system interpolates between the $N_h + N_\ell = 12$ flavor mass deformed conformal and the $N_\ell = 4$ chirally broken models. Effectively we replace the discrete flavor number by a

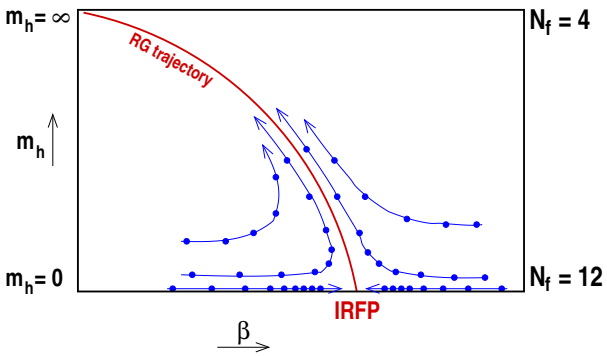

Figure 1: Illustration of the expected renormalization group flow lines for the $N_\ell + N_h$ flavor theory. The red line shows the RG trajectory connecting the conformal IRFP at $m_h = m_\ell = 0$ (12 flavors) and the trivial fixed point of the 4-flavor theory at $m_h = \infty$. The blue lines are RG flow lines that first approach, then run along the RG trajectory. As $m_h \to 0$ the flow lines spend increasingly more time around the IRFP, creating a "walking" scenario, while as m_h increases the heavy flavors decouple and the RG flows resemble the running of the 4-flavor system.

continuous mass parameter m_h.

In Figure 1 we sketch the renormalization group (RG) flow of the $N_\ell + N_h$ model in the limit $m_\ell = 0$. In this system the mass m_h of the heavy fermion is a relevant parameter. If $m_h > 0$ the RG transformation traces out a trajectory that runs from the IRFP of the massless 12-flavor theory towards the trivial fixed point of the massless 4-flavor theory. For large m_h the heavy fermions decouple and the system resembles the 4-flavor chirally broken theory, while in the limit of vanishing $m_h = m_\ell = 0$ it is conformal with the RG flow running into the IRFP. By tuning the mass of the heavy fermions we can control the RG flow that first approaches the IRFP, stays there for a while, and eventually runs toward the trivial fixed point. In this setup we control the "length" of walking by tuning the heavy mass m_h, interpolating between the 12-flavor mass-deformed conformal system in the ultraviolet and the 4-flavor chirally broken one in the infrared.

We chose to simulate a theory with 4+8 flavors because this is the natural choice when using staggered fermions. This system might not be the most promising BSM candidate. Simulating, e.g., a theory with $2+1$ flavors of sextet fermions could be phenomenologically more interesting since that system would have only three massless Goldstone bosons as suggested by electroweak symmetry breaking. Also, there is increasing evidence that the $SU(3)$ 12-flavor system has a relatively small $\gamma_m^\star \approx 0.24$ anomalous dimension [13, 15, 20] which may be insufficient to satisfy phenomenological walking constraints. A system with a larger anomalous dimension might be more realistic. However using 4+8 flavor staggered fermions allows us to embed this project into a larger program studying many flavor $SU(3)$ theories based on simulations with the same gauge and fermion action [10, 13, 14, 20–23].

In the following Section we will first provide details on our numerical simulations and briefly discuss properties of the generated ensembles. In Section 3 we present our preliminary results for determining the running coupling. As expected we observe a walking behavior in dependence of the heavy mass m_h. Aiming to explore the effect of a walking coupling on the "meson spectrum" of our theory, we show our preliminary findings based on connected and disconnected measurements

Table 1: Overview of our currently available ensembles at $\beta = 4.0$ for up to five different values of the light quark mass m_ℓ and three different values for the heavy quark mass m_h. The table names the number of thermalized configurations, the HMC acceptance rate, and the Wilson flow scale $\sqrt{8\tilde{t}_0}$ for each ensemble. Configurations are saved every 10 trajectories and 1 trajectory = 1 MDTU. $^\heartsuit$ indicates HMC runs currently in progress; $^\clubsuit$ marks ensembles with ongoing measurements.

		$m_h = 0.060$			$m_h = 0.080$			$m_h = 0.100$		
$L^3 \times T$	m_l	N_{config}	Acc.	$\sqrt{8\tilde{t}_0}$	N_{config}	Acc.	$\sqrt{8\tilde{t}_0}$	N_{config}	Acc.	$\sqrt{8\tilde{t}_0}$
$24^3 \times 48$	0.005	1000	85.8%	7.86(4)	1000	85.4%	6.11(1)	1000	85.6%	4.939(6)
$24^3 \times 48$	0.010	1000	85.3%	7.14(3)	1000	85.9%	5.72(1)	1000	86.1%	4.673(6)
$24^3 \times 48$	0.015	1026	93.1%	6.74(2)	1000	86.1%	5.415(8)	1000	85.7%	4.449(5)
$24^3 \times 48$	0.025	1065	93.2%	5.98(1)	1020	85.1%	4.962(6)	1010	85.7%	4.082(4)
$24^3 \times 48$	0.035	1053	93.1%	5.65(1)	1020	85.1%	4.587(4)	1026	84.2%	3.785(3)
$32^3 \times 64$	0.005	$1015^\clubsuit$	76.8%	7.65(2)	$841^{\heartsuit\clubsuit}$	85.0%	6.093(9)	$140^{\heartsuit\clubsuit}$	79.8%	4.94(1)
$32^3 \times 64$	0.010	$1009^\clubsuit$	77.0%	7.16(2)	$1010^\clubsuit$	89.3%	5.70(6)	$140^{\heartsuit\clubsuit}$	89.9%	4.674(8)

in Section 4 before we finally conclude.

2. Numerical setup

We perform our simulations using the combination of nHYP [24] smeared staggered fermions and the plaquette gauge action with fundamental and adjoint terms [13, 25]. This action with various numbers of fermion flavors has been used in numerous other works (see e.g. [13, 25]). The nHYP smeared fermions have small taste breaking and simulations with our choice of smearing parameters are numerically stable. Our ensembles of gauge field configurations are generated using the hybrid Monte Carlo (HMC) update algorithm [26] as implemented in the FUEL software package [27]. We contributed our own measurement code for the connected and disconnected meson spectrum to this software project.

After an initial study with two values for the gauge coupling β, we fixed $\beta = 4.0$ ($\beta_a = -\beta/4$ [28]) to perform our first study of the running coupling and the meson spectrum as a function of the heavy quark mass m_h. We present results obtained at two different lattice volumes, $L^3 \times T = 24^3 \times 48$ and $32^3 \times 64$, with three different values for the heavy quark m_h and up to five different values for the light quark m_ℓ. We summarize our currently available configurations in Table 1. Work is however in progress and we are extending some of the existing ensembles as well as increasing the number of measurements, in addition to planning new simulations at different mass values.

In total this work utilizes 21 ensembles which we present in a graphical overview in Fig. 2. The plot on the left visualizes our $24^3 \times 48$ and $32^3 \times 64$ ensembles in the parameter-space spanned by m_ℓ and m_h. There we also try to characterize the quality of the ensemble with respect to finite size effects using a color coding from green (no visible effects), over orange to red (severe finite size effects). Please note however this color coding is somewhat ad hoc and may need to be revisited in the future. The right plot shows the t-shift improved gradient flow scale $\sqrt{8\tilde{t}_0}$ vs. m_ℓ for our 21 ensembles. (Details on the gradient flow and the definition of the t-shift improved scale $\sqrt{8\tilde{t}_0}$ are given in the following section.) Chirally extrapolating in the light quark mass m_ℓ, i.e. focusing

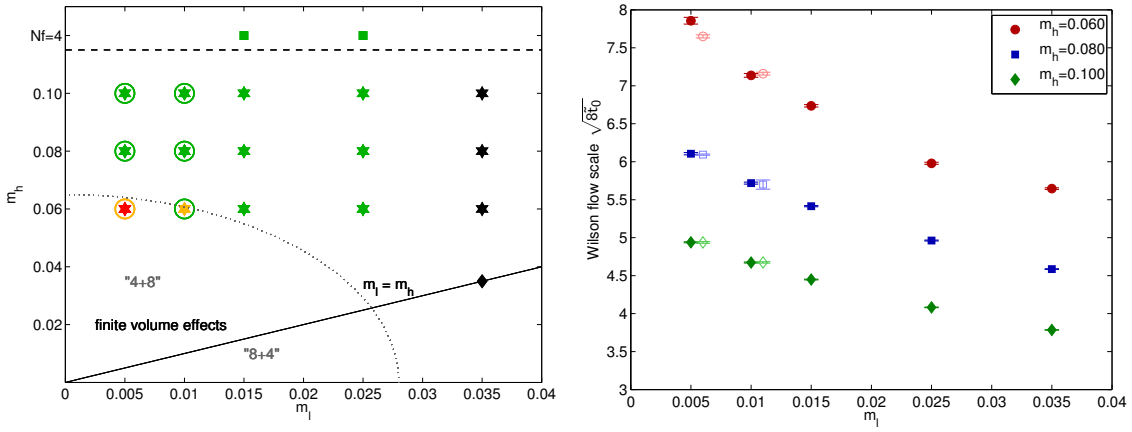

Figure 2: Left panel: light (m_ℓ) and heavy (m_h) mass values for the simulations carried out on $24^3 \times 48$ lattices (filled symbols) and $32^3 \times 64$ lattice (open circles). The colors are meant to caution about finite size effects, likely negligible for green, but of increasing importance as the color turns to orange and red. The black data points are likely too heavy and affected by cut-off effects. Right panel: The gradient flow scale $\sqrt{8\tilde{t}_0}$ for our 21 ensembles vs. m_ℓ. Filled symbols show values determined on $24^3 \times 48$ lattices, open symbols (shown with a small horizontal offset) refer to the values measured on $32^3 \times 64$ lattices. The strong dependence on both the heavy and light fermion masses is most likely the effect of the IRFP of the 12 flavor system.

on data with the same m_h (same symbol/color), we observe a non-linear increase of $\sqrt{8\tilde{t}_0}$ as m_ℓ decreases. Moreover, we find a strong dependence on m_h resulting in a larger scale $\sqrt{8\tilde{t}_0}$ with decreasing m_h. How finite volume affects $\sqrt{8\tilde{t}_0}$ can be seen by comparing filled ($24^3 \times 48$ data) and open symbols ($32^3 \times 64$ data) with each other. For better visibility, $32^3 \times 64$ data are shown with a small horizontal offset. In case of the gradient flow scale $\sqrt{8\tilde{t}_0}$ significant finite size effects are only present for our lightest data point with $m_\ell = 0.005$ and $m_h = 0.060$.

The strong dependence of the gradient flow scale on our input parameters m_ℓ and m_h may give rise to concerns about the quality of our ensembles in particular for lighter masses m_ℓ and m_h. In order to obtain one measure on the quality, we study the evolution of the topological charge as a function of the Molecular Dynamics time τ. We measure the topological charge on configurations smoothed by gradient flow transformations at flow time $t = 18.0$ using an $O(a^4)$-improved definition of the topological charge

$$Q = \frac{g^2}{32\pi^2} \sum_x \varepsilon_{\mu\nu\rho\sigma} \mathrm{Tr}\left\{ F_{\mu\nu}(x) F_{\rho\sigma}(x) \right\}, \tag{2.1}$$

where $F_{\mu\nu}(x)$ is an appropriate linear combination of 1×1, 2×2, and 3×3 clover-leaf Wilson loops as defined in [29].

In all cases we find that the topological charge is tunneling well; we are sampling different topological sectors with an average net topological charge of near zero. As expected, by going to smaller values of m_ℓ and m_h we do observe slower tunneling and the topological charge fluctuates with a smaller amplitude. Both leads to an increase of the integrated autocorrelation time. As an example we show in Fig. 3 plots for the evolution of the topological charge on our 24^3 ensembles with $m_\ell = 0.010$ and $m_h = 0.060, 0.080, 0.100$.

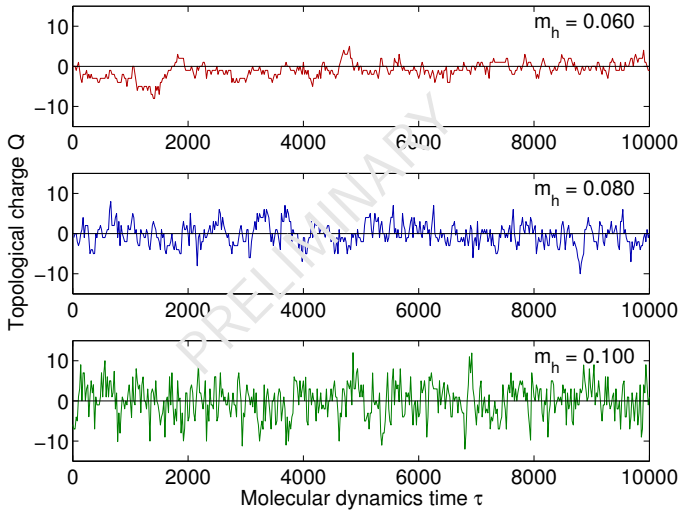

Figure 3: Topological charge as function of the Molecular Dynamics time τ for our three $24^3 \times 48$ ensembles with $m_\ell = 0.010$ and $m_h = 0.060$, 0.080, 0.100. As we reduce the heavy mass m_h, slower tunneling of the topological charge and a smaller range of fluctuations occur.

3. Running Coupling

3.1 Scale setting using Wilson flow

The gradient flow is an invertible and continuous smearing transformation of the gauge field. It systematically removes cut-off effects and can therefore be used to define renormalized quantities, like the gradient flow renormalized running coupling [30–32]

$$g^2_{GF}(\mu) = \frac{1}{\mathcal{N}} \langle t^2 E(t) \rangle. \tag{3.1}$$

The flow time $t = a^2 t_{\text{lat}}$, $t_{\text{lat}} \gg 1$, defines the energy scale $\mu^{-1} = \sqrt{8t}$ and the energy density

$$E(t) = -\frac{1}{2} \text{ReTr}[G_{\mu\nu}(t) G^{\mu\nu}(t)] \tag{3.2}$$

can be evaluated by any appropriate lattice operator. The constant $\mathcal{N} = 3(N^2-1)/128\pi^2$ is chosen such that g^2_{GF} matches the traditional $\overline{MS}$ coupling in perturbation theory [32].

By fixing the value of the running coupling one can define a lattice scale t_c

$$g^2_{GF}(t_c) = \frac{c}{\mathcal{N}}. \tag{3.3}$$

In this work we use the t_0 scale introduced in [32] which corresponds to $c = 0.3$. There is the freedom to chose c differently and we will come back to that later.

At finite lattice spacing g^2_{GF} has cut-off corrections that, for staggered fermions, are expected to be $\mathcal{O}(a^2)$

$$g^2_{\text{GF}}(\mu; a) = g^2_{\text{GF}}(\mu; a = 0) + a^2 \mathscr{C} + \mathcal{O}(a^4 [\log a]^n, a^4). \tag{3.4}$$

The term $a^2\mathscr{C}$ depends on the action, the flow transformation, and the operator used to evaluate $E(t)$ in Eq. (3.2). It can be significant on coarse lattices. Reference [14] suggested a simple, empirical

method to largely reduce cut-off corrections by replacing $g^2_{\rm GF}(\mu;a)$ with

$$\widetilde{g}^2_{\rm GF}(\mu;a) = \frac{1}{\mathcal{N}}\langle t^2 E(t+\tau_0 a^2)\rangle, \tag{3.5}$$

where $\tau_0 \ll t/a^2$ is a small finite shift in the flow time. In the continuum limit $\tau_0 a^2 \to 0$ and $\widetilde{g}^2_{\rm GF}(\mu) = g^2_{\rm GF}(\mu)$. At finite lattice spacing it is possible to choose τ_0 such that the $a^2\mathscr{C}$ term in Eq. (3.4) is canceled and

$$\widetilde{g}^2_{\rm opt}(\mu;a) = g^2_{\rm GF}(\mu;a=0) + \mathcal{O}(a^4[\log a]^n, a^4). \tag{3.6}$$

For full $\mathcal{O}(a^2)$ improvement the t-shift τ_0 must depend on both the bare and renormalized coupling. In practice it is sufficient to choose τ_0 to be a constant or only weakly dependent on $\widetilde{g}^2_{\rm GF}(\mu)$ to remove most $\mathcal{O}(a^2)$ lattice artifacts. Refs. [33, 34] demonstrated that the t-shift improvement with constant τ_0 removes most lattice artifacts of the t_0 scale when using the 2+1+1 flavor HISQ action.

The reduction of lattice artifacts is particularly important in the present work as with only one gauge coupling we are not able to take a proper continuum limit. To illustrate the cut-off effects we show the unshifted $g^2_{\rm GF}(t)$ couplings of the $m_h = 0.060$, 0.080 and 0.100 systems in the left panel of Fig. 4. We use data from our $32^3 \times 64$ volumes with the light fermion mass extrapolated to the chiral limit $m_\ell \to 0$, and rescale the gradient flow time t by the scale factor t_0. The rapid rise of $g^2_{\rm GF}(t)$ at small t is due to the initial integration of the gradient flow and can be considered an UV cut-off effect. Beyond this initial rise, in the intermediate energy regime the gradient flow coupling is influenced by the IRFP of the $N_f = 12$ flavor system and can be different for different m_h values. As the energy scale decreases further the heavy flavors decouple, and the running couplings of all three systems follow that of the $N_f = 4$ model. Assuming the t_0 scale is already in the IR regime, we expect that the renormalized couplings are t independent when $t/t_0 \gtrsim 1$. This is obviously not the case on the left panel of Fig. 4, signaling the presence of cut-off effects in $g^2_{\rm GF}$.

A small τ_0 shift can reduce the cut-off effects. A possible way to find the optimal τ_0 parameter is to require that the relative scales of the different m_h systems are independent of the specific choice of the parameter c in Eq. (3.3). By comparing two different values, $c = 0.3$ and $c = 0.35$, we find $\tau_{\rm opt} \approx 0.1$ to be optimal. The coupling $\widetilde{g}^2_{\rm GF}$ with this choice becomes largely independent of $\tilde{t}$ as the right panel of Fig. 4 shows. The small deviation observed at large $\tilde{t}/\tilde{t}_0$ is due to finite volume effects, but apart from that the three systems predict the same renormalized running coupling for $t/t_0 \gtrsim 0.3$. This implies the corresponding scales, denoted by $\tilde{t}_c$, have small cut-off effects. Even though the optimal t-shift was predicted in the chiral limit, we expect the same value to be also close to optimal at finite m_ℓ [33]. We compare the lattice scales of our different ensembles on the right panel of Fig. 2 where we show the t-shifted $\sqrt{8\tilde{t}_0}$ in lattice units from our $24^3 \times 48$ and $32^3 \times 64$ volume simulations. To control finite volume effects $\sqrt{8t_0} \lesssim L/5$ is usually sufficient. This appears to be true in our case as can be seen in Fig. 2 or by comparing the values in Table 1. We also find relatively strong dependence of $\sqrt{8\tilde{t}_0}$ on the light mass m_ℓ indicating that we might need larger volumes when taking the $m_\ell \to 0$ chiral limit.

3.2 Defining the running coupling from Wilson flow

The t-shift improved gradient flow coupling can be used to monitor the energy dependence of the running coupling. Figure 5 shows $\widetilde{g}^2_{\rm GF}(\mu)$ as the function of the energy μ for our three

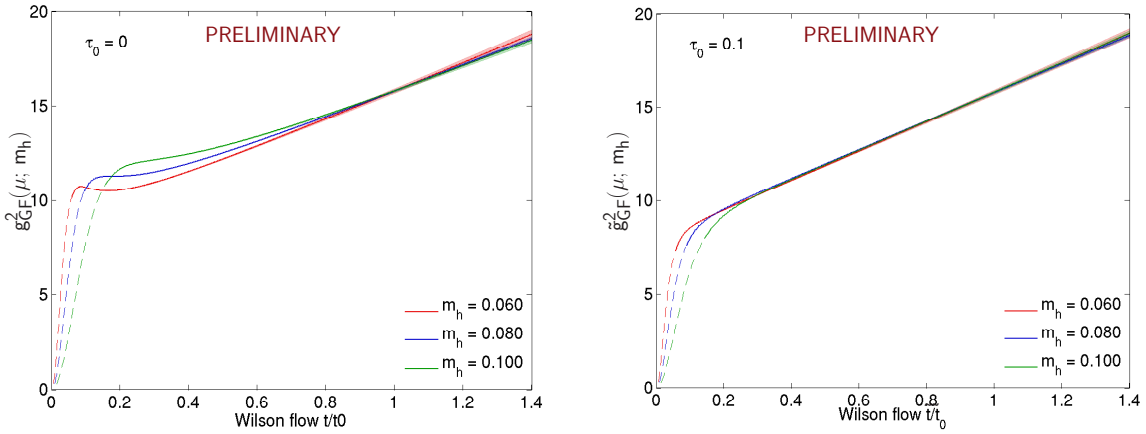

Figure 4: Left panel: the gradient flow coupling $g^2_{\rm GF}(t)$ for different values of m_h with m_ℓ extrapolated to the chiral limit. The different data sets are rescaled with their corresponding t_0 value. Right panel: like on the left but for the improved $\tilde{g}^2_{\rm GF}(t)$ coupling with $\tau_0 = 0.1$. The dashed sections of the lines indicate where we suspect cut-off effects may be significant.

$N_f = 4+8$ flavor ensembles and for an $N_f = 4$ flavor system as well. In all cases the light masses are extrapolated to the chiral limit and we rescale μ by the lattice scale $\mu_0^{-1} = \sqrt{8\tilde{t}_0}$. Figure 5 is basically the same as the right panel of Fig. 4 but replacing $\tilde{t}$ with μ reveals important features of the running coupling. At large μ the gradient flow coupling is dominated by lattice artifacts. In this region, where $\sqrt{8\tilde{t}_{\rm lat}} \lesssim 2.0$, we use dashed lines both in Fig. 4 and 5. In the IR limit at small μ the different systems predict a unique curve corresponding to the running coupling of the 4-flavor system. There is a clear intermediate energy region where the running coupling depends strongly on the heavy mass m_h. While the $N_f = 4$ system shows the expected fast running, as m_h decreases a shoulder develops. This is the walking behavior sought for in BSM systems. The width of the shoulder that is related to the length in energy of slow running can be tuned by tuning $m_h \to 0$, as we discussed in detail in Sec. 1.

It is important to monitor the evolution of the mass anomalous dimension. This can be done using the mode number of the Dirac operator [20, 25]. Our preliminary results indicate a reasonably large anomalous dimension. The details of that calculation will be reported in a forthcoming publication.

4. Light flavor spectrum

In Section 3 we demonstrated that by tuning the mass of the heavy fermions of the $4+8$ flavor system we can control the running and extend the walking nature of the renormalized coupling, an important component of many BSM models. In this section we turn our attention to the spectrum of the light flavors. We are especially interested in the mass of the 0^{++} iso-singlet light flavor scalar state, and its dependence on the dynamical heavy flavors. Even with our currently limited statistics, the connected spectrum is well controlled. For the 0^{++} state, however, we present only results at a single m_h value.

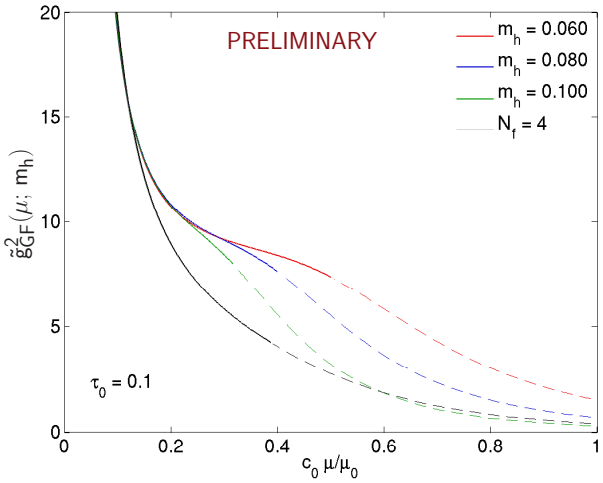

Figure 5: The running coupling constant $\tilde{g}^2_{\rm GF}$ at the mass scale μ for different values of m_h with m_ℓ extrapolated to the chiral limit. μ_0 and $c_0 = \mu_0^{-1}|_{m_h=0.060}$ serve as normalization constants that ensure that the different systems are compared at matching energy scales and τ_0 is the shift parameter to remove discretization errors. The dashed sections of the lines indicate where we suspect cut-off effects may be significant.

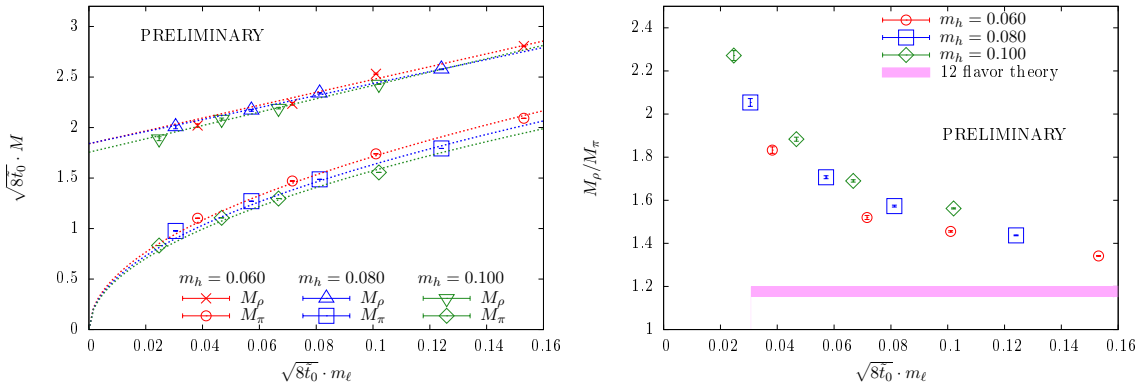

Figure 6: Left panel: the pion and rho meson masses as the function of the light fermion mass. All masses are in units of the gradient flow scale $\sqrt{8\tilde{t}_0}$ (see Table 1). The dashed lines serve to guide the eye indicating the expected chiral extrapolation: linear for the masses of the rho-meson and proportional to $\sqrt{m_\ell}$ for the pion masses. Right panel: the ratio M_ρ/M_π as the function of the light fermion mass. The shaded band around 1.17 indicates the value in the $m_h = m_\ell$ 12-flavor limit.

A phenomenologically relevant BSM model should predict a light iso-singlet scalar in the chiral limit, while all other non-Goldstone hadronic states remain heavy. We would like to understand if such a spectrum is possible in our model and how tuning the heavy flavors affects it. It is useful to recall what is known about the meson spectrum of the $N_f = 12$ system, the limiting case when $m_h \to m_\ell$. In conformal systems near the chiral limit the masses of hadronic states scale with $\gamma^\star_m$,

the anomalous dimension of the corresponding IRFP

$$M_H \propto m^{1/(1+\gamma_m^*)} + \text{corrections}. \tag{4.1}$$

When the corrections that are due to the irrelevant gauge coupling and/or large fermion mass, become negligible, the ratio of any two hadronic states becomes independent of the fermion mass. In the 12-flavor system, where the gauge coupling is nearly marginal, corrections to the scaling can be significant. Different staggered lattice actions at various values of the gauge coupling predict the ratio of M_ρ/M_π between 1.0 and 1.25 [11, 13, 15]. For our action at gauge coupling $\beta = 4.0$ the ratio is ≈ 1.17 and due to corrections to scaling decreases slightly toward the chiral limit.

In the $N_\ell = 4$ system chiral symmetry is spontaneously broken. The Goldstone boson mass scales as $M_\pi^2 \propto m_\ell$, while all other hadronic states remain massive in the chiral limit. The ratio M_ρ/M_π diverges as $m_\ell^{-1/2}$, in sharp contrast to conformal systems.

Our results in the 4+8 flavor system for the pion and rho are consistent with spontaneous chiral symmetry breaking. For illustration in the left panel of Fig. 6 we show the pion and rho spectrum for $m_\ell = 0.005$, 0.010, 0.015 and 0.025 for all three m_h values. Since the lattice scale $\tilde{t_0}$ shows strong dependence on both the heavy and light fermion masses (see the right panel of Fig. 2), we rescale the lattice masses in Fig. 6 by t-shift improved $\sqrt{8\tilde{t_0}}/a$ as listed in Table 1. Results presented in this figure were obtained on the largest volume available at each mass (see Table 1). Based on the comparison of the spectrum on $24^3 \times 48$ and $32^3 \times 64$ volumes, we expect small to negligible finite volume effects for every data point with the possible exception of $m_\ell = 0.005$, $m_h = 0.060$. It is surprising how independent the rho spectrum is of the heavy fermion mass. The pion shows more variation that is further enhanced on the right panel of Fig. 6 where we look at the ratio M_ρ/M_π as function of the rescaled light fermion mass. This indicates the heavy mass influences the continuum limit even for these very basic infrared quantities. Nevertheless all three m_h data sets show a rapid increase in this ratio as the light fermion mass approaches the chiral limit, as opposed to the magenta band which indicates the range M_ρ/M_π takes in the 12 flavor system. We do not show explicit mass dependence for $N_f = 12$ as the concept of a lattice scale and the quantity $\sqrt{8t_0}/a$ are not well defined for a conformal system. Fortunately M_ρ/M_π varies little with the fermion mass and the band in Fig. 6 is representative of its value.

The most interesting spectral quantity, the iso-singlet 0^{++} σ meson mass, is considerably more difficult to extract than the non-singlet mesons as it requires the evaluation of disconnected diagrams. Recent results [16–18] suggest that in conformal and near-conformal systems the 0^{++} mass can be relatively light, making it somewhat easier to obtain in numerical simulations. The 0^{++} correlator is a combination of connected and disconnected diagrams

$$C_{0^{++}}(t) \equiv \frac{N_\ell}{4} C_{\text{disc}}(t) - C_{\text{conn}}(t), \tag{4.2}$$

where the disconnected part is constructed from the vacuum subtracted operator $\langle\bar{\psi}\psi\rangle(t) - \langle\langle\bar{\psi}\psi\rangle\rangle_{\text{e}}$, and $\langle\langle\bar{\psi}\psi\rangle\rangle_{\text{e}}$ denotes the ensemble average of the fermion condensate. We construct the operator $\langle\bar{\psi}\psi\rangle(t)$ using N_{r} full volume noise sources $\eta_i(\vec{x},t)$ satisfying

$$\lim_{N_r\to\infty} \frac{1}{N_r} \sum_i \eta_i^\dagger(\vec{x},t)\eta_i(\vec{y},t') = \delta_{\vec{x},\vec{y}}\delta_{t,t'}\,. \tag{4.3}$$

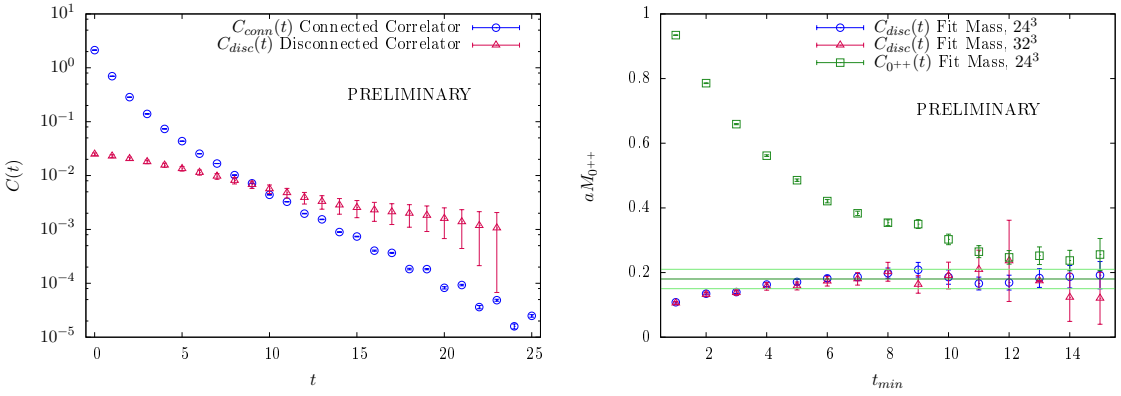

Figure 7: Left panel: Comparison of $C_{\text{conn}}(t)$ and $C_{\text{disc}}(t)$ for the $32^3 \times 64$ $m_\ell = 0.010$, $m_h = 0.060$ ensemble, showing that $C_{\text{conn}}(t)$ dominates the $C_{0^{++}}$ correlator for small t, while for larger t the noise overwhelms the $C_{\text{disc}}(t)$ correlator. Right panel: Predictions for the 0^{++} mass for $m_\ell = 0.010$, $m_h = 0.060$. The results are from correlated fits with a non-oscillating plus oscillating terms in the range of t_{min} and $N_t/2$. We show results both for $24^3 \times 48$ and $32^3 \times 64$ volumes when fitting the disconnected correlator only and $24^3 \times 48$ volume results when the correlator $C_{0^{++}}$ is considered.

By inverting the staggered Dirac matrix $D((\vec{x},t),(\vec{y},t'))$ we obtain

$$\phi_i(\vec{x},t) = D((\vec{x},t),(\vec{y},t'))^{-1}\eta_i(\vec{y},t') \tag{4.4}$$

which leads to the scalar operator

$$\langle\bar{\psi}\psi\rangle(t) = \lim_{N_r\to\infty}\frac{1}{N_r}\sum_i\sum_{\vec{x}}\eta_i^\dagger(\vec{x},t)\phi_i(\vec{x},t). \tag{4.5}$$

On each configuration we use $N_{\text{r}} = 6$ full volume $U(1)$ noise sources diluted in time, color, as well as even/odd in space to reduce stochastic noise [35]. To further enhance our signal, we use an improved operator for the chiral condensate, unique to naïve and staggered fermions, which replaces $\phi\eta$ in Equation (4.5) with $m\phi\phi$.

We compare the connected and disconnected scalar correlators on the left panel of Fig. 7 for the $32^3 \times 64$, $m_\ell = 0.010$, $m_h = 0.060$ ensemble. At present we have evaluated the disconnected correlator on only 89 configurations and we lose the signal in the noise for large t. Nevertheless the structure of the correlators is clear: For small t the connected correlator dominates the combination $C_{0^{++}}$ in Eq. (4.2), the effect of the disconnected contribution does not appear until $t \gtrsim 8$. Unfortunately by that time the signal of C_{disc} is very noisy and we are not able to identify a reliable plateau in the mass. An alternative, advocated by Refs. [16–18], is to consider the disconnected correlator only. As long as it couples to the 0^{++} state and that state is the lightest in the channel, the iso-singlet scalar mass can be extracted from the C_{disc} correlator alone. In practice, the disconnected correlator works even better, as apparently the excited state contributions in the connected and 0^{++} correlators cancel. The oscillating partner, clearly visible in the connected correlator in Fig. 7, is also suppressed in C_{disc} possibly because the splitting between the iso-singlet and non-singlet partner pions is small. However, it is not absent and we observe its presence even after parity pro-

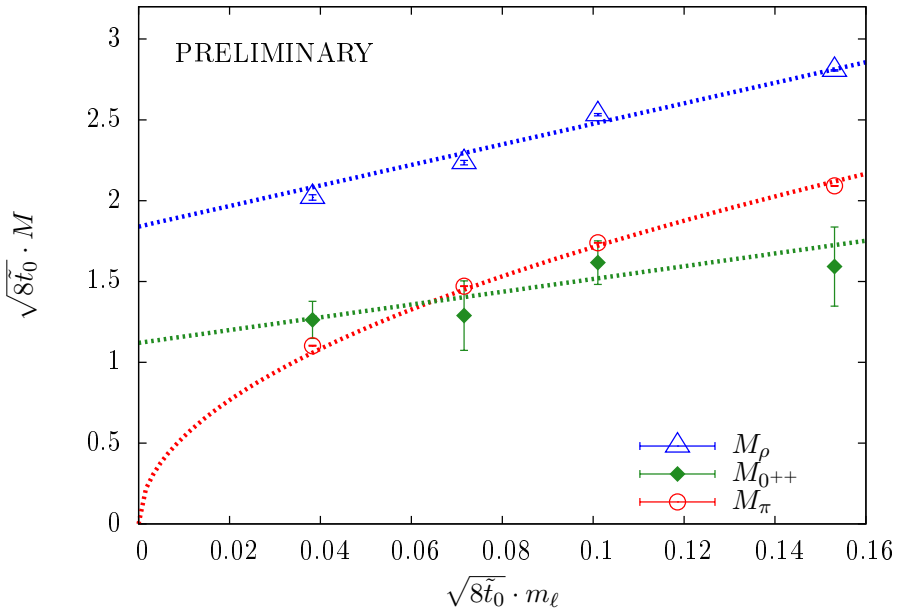

Figure 8: The pion, rho and 0^{++} scalar light flavor spectrum for $m_h = 0.060$.

jecting the correlator. We found it more reliable to extract the 0^{++} mass from a correlated fit using a combination of non-oscillating and an oscillating terms.

The right panel of Fig. 7 shows the 0^{++} mass as predicted by such correlated fits at $m_\ell = 0.010$, $m_h = 0.060$. The largely overlapping red and blue symbols correspond to predictions obtained on the $24^3 \times 48$ and $32^3 \times 64$ ensembles, respectively. In both cases we fit the disconnected correlator C_{disc} between time slices t and $t_{\text{max}} = N_t/2$. Predictions from the two volumes agree within errors and a plateau predicting $M_{0^{++}} = 0.18(3)$ develops for $t \gtrsim 7$. We also show in the figure the predictions from the $C_{0^{++}}$ correlator of Eq. (4.2). The mass of the connected a_0 scalar on these ensembles is $M_{a_0} = 0.360(3)$ but the connected correlator couples strongly to excited states and we do not observe a plateau even when fitting only C_{conn} until $t \gtrsim 13$. The excited state contribution carries over to the $C_{0^{++}}$ correlator and the predicted mass drops steadily up to $t = 12$. The plateau that conceivably develops for larger t is within errors consistent with the prediction obtained form the disconnected correlator only.

Finally, in Fig. 8 we show our preliminary results for the pion, rho and 0^{++} scalar light flavor spectrum for the ensembles with $m_h = 0.060$. As in Fig. 6 we express all masses in terms of the gradient flow scale $\sqrt{8\tilde{t}_0}$. At the lightest mass we use $32^3 \times 64$ volumes, but even that could be volume squeezed. At all other mass values we found only small deviations between $24^3 \times 48$ and $32^3 \times 64$. Like in the studies of conformal or near-conformal systems in Refs. [16–18], our isosinglet scalar is light, below the pion at the three heavier mass values. At the lightest mass the scalar state is above the pion, but the difference is not statistically significant. Since finite volume effects make the pion heavy and appear to make the 0^{++} scalar light [16, 17], this difference could increase on larger volumes. In a spontaneously chirally broken system we expect the scalar mass to remain finite in the chiral limit and our data are consistent with a linear mass dependence. Our

preliminary results suggests $m_\rho/m_\sigma \approx 1.7$ in the chiral limit. We want to emphasize that the results for the disconnected scalar are preliminary, based on relatively low statistics and a subset of our ensembles. However if our findings remain unchanged, to our knowledge this is the first time that the iso-singlet scalar mass is observed to cross the pion; the data presented in Refs. [16–18] show the iso-singlet scalar to stay below or indistinguishable from the pion.

5. Conclusions and outlook

Gauge-fermion systems near the conformal window are interesting not only as strongly coupled field theory models but could also have important phenomenological applications. In recent years many large-scale lattice studies have began to investigate systems with different gauge groups, fermion representations, and fermion numbers with the goal of identifying the onset of conformal behavior and investigating the properties of systems just below the conformal window. These investigations are, however, limited by an integer number of flavors. Our model avoids that limitation by simulating four light and eight heavy flavors where the mass of the heavy flavors is a continuous parameter allowing us to tune arbitrarily close to the conformal fixed point of the 12-flavor system in the ultraviolet, while still describing chirally broken four light flavors in the infrared limit.

We use this setup to study the energy dependence of the gauge coupling and confirm numerically a theoretically expected walking behavior. We also demonstrate that the length of walking (energy) can be changed by varying the mass of the heavy flavors. In addition, we compute the meson spectrum of the light flavors with special emphasis on the 0^{++} scalar. Our preliminary results reveal an iso-singlet scalar that is lighter than the pion at large fermion mass but becomes heavier at smaller masses. Further simulations will have to confirm our current findings. Measurements of the disconnected correlator are in progress on the other ensembles. While we might not be able to extract the mass of the 0^{++} state at larger m_ℓ values, we expect to be able to determine the mass of the iso-singlet scalar at least at the lightest m_ℓ values for each m_h ensemble. It would also be very interesting to study even lighter m_ℓ values, possibly on larger volumes, to firmly establish the chiral behavior of the iso-singlet scalar compared to the Goldstone pion. Some of these investigations are under way and will be presented in a future publication.

Acknowledgments

Computations for this work were carried out in part on facilities of the USQCD Collaboration, which are funded by the Office of Science of the U.S. Department of Energy, on computers at the MGHPCC, in part funded by the National Science Foundation, and on computers allocated under the NSF Xsede program to the project TG-PHY120002.
We thank Boston University, Fermilab, the NSF and the U.S. DOE for providing the facilities essential for the completion of this work. R.C.B., C.R. and E.W. were supported by DOE grant DE-SC0010025. In addition, R.C.B., C.R. and O.W. acknowledge the support of NSF grant OCI-0749300. A.H. acknowledges support by the DOE grant DE-SC0010005.

References

[1] G. Aad et al. (ATLAS Collaboration), Phys.Lett. **B716**, 1 (2012), arXiv:1207.7214 [hep-ex] .
[2] S. Chatrchyan et al. (CMS Collaboration), Phys.Lett. **B716**, 30 (2012), arXiv:1207.7235 [hep-ex] .
[3] S. Weinberg, Phys.Rev. **D19**, 1277 (1979).
[4] L. Susskind, Phys.Rev. **D20**, 2619 (1979).
[5] S. Dimopoulos and L. Susskind, Nucl.Phys. **B155**, 237 (1979).
[6] E. Eichten and K. D. Lane, Phys.Lett. **B90**, 125 (1980).
[7] K. Yamawaki, M. Bando, and K.-i. Matumoto, Phys. Rev. Lett. **56**, 1335 (1986).
[8] T. Appelquist, J. Terning, and L. C. R. Wijewardhana, Phys. Rev. D **44**, 871 (1991).
[9] T. Appelquist, G. Fleming, M. Lin, E. Neil, and D. Schaich, Phys.Rev. **D84**, 054501 (2011), arXiv:1106.2148 [hep-lat] .
[10] A. Hasenfratz, Phys.Rev.Lett. **108**, 061601 (2012), arXiv:1106.5293 [hep-lat] .
[11] Y. Aoki, T. Aoyama, M. Kurachi, T. Maskawa, K.-i. Nagai, et al., Phys.Rev. **D86**, 054506 (2012), arXiv:1207.3060 [hep-lat] .
[12] T. DeGrand, Phys.Rev. **D84**, 116901 (2011), arXiv:1109.1237 [hep-lat] .
[13] A. Cheng, A. Hasenfratz, Y. Liu, G. Petropoulos, and D. Schaich, Phys.Rev. **D90**, 014509 (2014), arXiv:1401.0195 [hep-lat] .
[14] A. Cheng, A. Hasenfratz, Y. Liu, G. Petropoulos, and D. Schaich, JHEP **1405**, 137 (2014), arXiv:1404.0984 [hep-lat] .
[15] M. Lombardo, K. Miura, T. J. N. da Silva, and E. Pallante, (2014), arXiv:1410.0298 [hep-lat] .
[16] Y. Aoki, T. Aoyama, M. Kurachi, T. Maskawa, K.-i. Nagai, et al., Phys.Rev.Lett. **111**, 162001 (2013), arXiv:1305.6006 [hep-lat] .
[17] Y. Aoki et al. (the LatKMI Collaboration), Phys.Rev. **D89**, 111502 (2014), arXiv:1403.5000 [hep-lat] .
[18] Z. Fodor, K. Holland, J. Kuti, D. Nogradi, and C. H. Wong, PoS **LATTICE2013**, 062 (2014), arXiv:1401.2176 [hep-lat] .
[19] R. Brower, A. Hasenfratz, C. Rebbi, E. Weinberg, and O. Witzel, (2014), arXiv:1410.4091 [hep-lat] .
[20] A. Cheng, A. Hasenfratz, G. Petropoulos, and D. Schaich, JHEP **1307**, 061 (2013), arXiv:1301.1355 [hep-lat] .
[21] A. Cheng, A. Hasenfratz, and D. Schaich, Phys.Rev. **D85**, 094509 (2012), arXiv:1111.2317 [hep-lat] .
[22] D. Schaich (USBSM), PoS (2013), arXiv:1310.7006 [hep-lat] .
[23] A. Hasenfratz, D. Schaich, and A. Veernala, (2014), arXiv:1410.5886 [hep-lat] .
[24] A. Hasenfratz, R. Hoffmann, and S. Schaefer, JHEP **0705**, 029 (2007), arXiv:hep-lat/0702028 [hep-lat] .
[25] A. Cheng, A. Hasenfratz, G. Petropoulos, and D. Schaich, PoS **LATTICE2013**, 088 (2013), arXiv:1311.1287 [hep-lat] .
[26] S. Duane, A. Kennedy, B. Pendleton, and D. Roweth, Phys.Lett. **B195**, 216 (1987).
[27] J. Osborn et al., "Framework for unified evolution of lattices (FUEL)," .
[28] M. Hasenbusch and S. Necco, JHEP **0408**, 005 (2004), arXiv:hep-lat/0405012 [hep-lat] .
[29] S. O. Bilson-Thompson, D. B. Leinweber, and A. G. Williams, Annals Phys. **304**, 1 (2003), arXiv:hep-lat/0203008 [hep-lat] .
[30] R. Narayanan and H. Neuberger, JHEP **0603**, 064 (2006), arXiv:hep-th/0601210 [hep-th] .
[31] M. Lüscher, Commun.Math.Phys. **293**, 899 (2010), arXiv:0907.5491 [hep-lat] .
[32] M. Lüscher, JHEP **1008**, 071 (2010), arXiv:1006.4518 [hep-lat] .
[33] A. Hasenfratz, "Non-perturbative reduction of cut-off effects of the t_0, w_0 gradient flow scales," (2014), In preparation.
[34] A. Hasenfratz, "Improved gradient flow for step scaling function and scale setting," (2014), Talk presented at Lattice 2014.
[35] J. Foley, K. Jimmy Juge, A. O'Cais, M. Peardon, S. M. Ryan, et al., Comput.Phys.Commun. **172**, 145 (2005), arXiv:hep-lat/0505023 [hep-lat]